PHYSICAL REVIEW D **91,** 114011 (2015)

Soft edge of hadron scattering and minijet models for the total and inelastic *pp* cross sections at LHC and beyond

D. A. Fagundes[*]
Instituto de Física Teórica, UNESP, Rua Dr. Bento T. Ferraz, 271, Bloco II, 01140-070 São Paulo, São Paulo, Brazil

A. Grau[†]
Departamento de Física Teórica y del Cosmos, Universidad de Granada, 18071 Granada, Spain

G. Pancheri[‡]
INFN Frascati National Laboratories, Via E. Fermi 40, Frascati 00444, Italy

Y. N. Srivastava[§]
Physics Department, University of Perugia, 06123 Perugia, Italy

O. Shekhovtsova[¶]
Kharkov Institute of Physics and Technology, Akademicheskaya, 1, Kharkov 61108, Ukraine and Institute of Nuclear Physics Polish Polska Akademia Nauk ul. Radzikowskiego, 152 31-342 Krakow, Poland

(Received 3 April 2015; published 8 June 2015)

We show that the onset and rise of QCD minijets provide the dynamical mechanism behind the appearance of a *soft edge* in pp collisions around CERN intersecting storage rings (ISR) energies, and thus such a soft edge is *built in* our minijet model with soft gluon resummation. Here the model is optimized for the LHC at $\sqrt{s} = 7$, 8 TeV and predictions made for higher LHC and cosmic ray energies. Further, we provide a phenomenological picture to discuss the breakup of the total cross section into its elastic, uncorrelated, and correlated inelastic pieces in the framework of a one-channel eikonal function.

DOI: 10.1103/PhysRevD.91.114011 PACS numbers: 13.75.Cs, 13.85.-t

I. INTRODUCTION

This paper has three main objectives: (i) to clarify the role played by QCD minijets in the high energy behavior of total cross sections in reference to recent observation about the onset of an energy invariant *soft edge* [1] in pp collisions, around CERN intersecting storage rings (ISR) energies; (ii) to provide an update of our model predictions at $\sqrt{s} = 13$ and 14 TeV (LHC13 and LHC14) for proton-proton scattering, both for total [2] and inelastic [3] cross sections; and (iii) to apply our minijet model to the very high energy behavior that may be of utility for analyses of the particle production cross section in the realm of cosmic rays.

The paper is organized as follows. In Sec. II, we begin by showing how the notion of minijets in its simplest formulation when augmented by asymptotic freedom leads easily to the appearance of a threshold in the total cross section around $\sqrt{s} \simeq (10 \div 20)$ GeV. Through the use of current parton density functions (PDFs), we then show that the onset and the rise of the minijet cross section is behind the observation of the soft edge.

Having thus highlighted the role of the minijet phenomenon in view of the recent observation of an *edgelike* structure [1,4] occurring in hadronic collisions near $\sqrt{s} \simeq (10 \div 20)$ GeV, in Sec. III, we provide a brief description of the model we proposed quite a long time ago [5], which overcomes the main limitation of the minijet description, namely the violation of the Froissart bound, through soft gluon k_t resummation. We take the opportunity to optimize our predictions for both LHC and higher energy pp data extracted from cosmic rays and include recent results at $\sqrt{s} = 7$ and 8 TeV. We also indicate the uncertainty coming from different sets of PDFs entering the calculations.

In Sec. IV, we apply our model to inelastic scattering at LHC and discuss the role played by minijets in nondiffractive scattering. A breakup of the inelastic cross section in terms of its correlated and uncorrelated parts and the extraction of the measured elastic cross section is provided in detail for a one-channel eikonal formulation, alongside a comparison with all available data.

Our model is not in conflict with the dominant analytic description of the total and elastic cross section based on

[*]dfagundes@ift.unesp.br
[†]igrau@ugr.es
[‡]giulia.pancheri@lnf.infn.it
[§]yogendra.srivastava@gmail.com
[¶]olga.shekhovtsova@ifj.edu.pl

Regge–Pomeron models such as for instance Ref. [6] or [7]; rather, it provides an intuitive description of hadronic scattering in terms of low p_t collisions describable by perturbative QCD and soft gluon emission, for which a mixed approach, perturbative and nonperturbative, is required.

II. SOFT EDGE AND MINIJETS

These are two basic *facts* about the pp and $p\bar{p}$ total cross section:

(i) $\sigma_{\rm total}$ first decreases and then around $\sqrt{s} \simeq (10 \div 20)$ GeV rises as a function of the squared c.m. energy s.

(ii) $\sigma_{\rm total}$ asymptotically cannot rise faster than $\log^2[s/s_o]$.

Both phenomena have a physical interpretation in terms of QCD; the difficulty lies in a proper implementation of the second fact. We shall start, in this section, from the first fact, in particular the rise, which appears when gluon-gluon scattering becomes observable. This argument can be made quantitative.

At low c.m. energy, soft gluon emission accompanying nonperturbative effects decreases the cross section, while there are not enough perturbative gluons for beam-on-beam scattering. However, as the energy increases, more energy is available for gluon emission, and there is a nonzero probability for hard gluon-gluon scattering with the production of final state partons of $p_t \sim 1$ GeV. For such energy regions, the collision can be described by perturbative QCD through the asymptotic freedom expression for the coupling, $\alpha_{AF}(p_t^2)$, valid when $p_t^2 \gg \Lambda^2_{\rm QCD}$. The emission of hard gluons is a perturbative process, characterized by a $1/x \sim \sqrt{s}/(2p_t)$ parton spectrum. As the energy increases further, the cross section for collisions resulting with a final state parton with $p_t \gtrsim 1$ will start rising because of $1/x$ behavior, entering into a *high gluon luminosity* region. We see that the contribution to the total cross section from these hard collisions can become sizable and rising with energy when

$$1/x = \sqrt{s}/2p_t \gg 1 \quad \text{and} \quad p_t > 1 \text{ GeV}. \tag{1}$$

With the condition $p_t > 1$ GeV for the *asymptotic freedom condition* to be satisfied, and the rise starting when $x \ll 1$, for instance $\simeq$0.1–0.2, the turning point for the rise to start is for

$$\sqrt{s} \gtrsim (2/x) \text{ GeV} \tag{2}$$

$$\sqrt{s} \sim (10 \div 20) \text{ GeV} \tag{3}$$

as the data show. The transition from collisions which do not involve scattering of perturbative gluons, to a region dominated by minijets, is what is seen in the total cross section data and is discussed, in a somewhat different language, in Ref. [1].

The above argument can be made quantitative by calculating the bulk of perturbative gluon-gluon collisions, i.e. the minijet cross section. The minijet cross section is given by

$$\sigma^{AB}_{\rm jet}(s; p_{\rm tmin}) = \int_{p_{\rm tmin}}^{\sqrt{s}/2} dp_t \int_{4p_t^2/s}^{1} dx_1 \int_{4p_t^2/(x_1 s)}^{1} dx_2 \times \sum_{i,j,k,l} f_{i|A}(x_1, p_t^2) f_{j|B}(x_2, p_t^2) \frac{d\hat{\sigma}^{kl}_{ij}(\hat{s})}{dp_t}, \tag{4}$$

where $f_{i|A}(x_1, p_t^2)$ are the PDFs with i, j, k, l to denote the partons and x_1, x_2 to denote the fractions of the parent particle momentum carried by the parton. $\sqrt{\hat{s}} = \sqrt{x_1 x_2 s}$, $\hat{\sigma}$ are the center-of-mass energy of the two parton system and the hard parton scattering cross section, respectively. Following the argument given above, this expression sums only collisions with outgoing partons of momentum with $p_t > p_{\rm tmin}$, where $p_{\rm tmin}$ is defined as the region of validity of perturbative QCD; i.e. the coupling is given by the asymptotic freedom expression for running α_F. Different densities give rise to different energy dependence of the minijet cross section, as they differ in their very low-x behavior. In Fig. 1 we display the energy dependence of $\sigma_{jet}(s)$, with parameter choices corresponding to $p_{\rm tmin} \simeq 1$ GeV and different PDFs. We use leading-order (LO) current PDFs DGLAP evolved, from PDF libraries. A clear threshold behavior appears around ISR energies and confirms the minijet explanation of the soft edge; that is, for $\sqrt{s} \gtrsim$ 10–20 GeV the cross section rises mainly due to the energy evolution of the proton "radius," coming from emergent gluon-gluon hard scatterings.

For a fixed $p_{\rm tmin}$, these minijet cross sections rise as a power law, $s^{0.3–0.4}$, and, when included in the formalism for the total cross section, phenomenologically correspond to the hard Pomeron of Regge–Pomeron models.

For the transition to be at the $\sqrt{s}$ values as indicated by the rise of the cross section at ISR, the parameter $p_{\rm tmin}$ has to be roughly energy independent. This is in disagreement with other, typically Regge–Pomeron, formulations but is in agreement with the observation in Ref. [1] and confirms the finding of our model, which, from the very beginning, used a constant p_t value, labelled as $p_{\rm tmin}$, as a divider between scattering giving rise to minijets and nonperturbative scattering.

However, this poses a serious problem with the rigorous limits imposed on cross sections by the Froissart bound. In various minijet or Regge–Pomeron based models, this is the main reason to introduce an energy dependent $p_{\rm tmin}$. In so doing, however, not only is there no way to simply explain the soft edge as a fixed energy threshold, but an important piece of physics remains hidden, namely soft gluon resummation that tames the unphysical rise of the minijet cross section, to which we now turn.

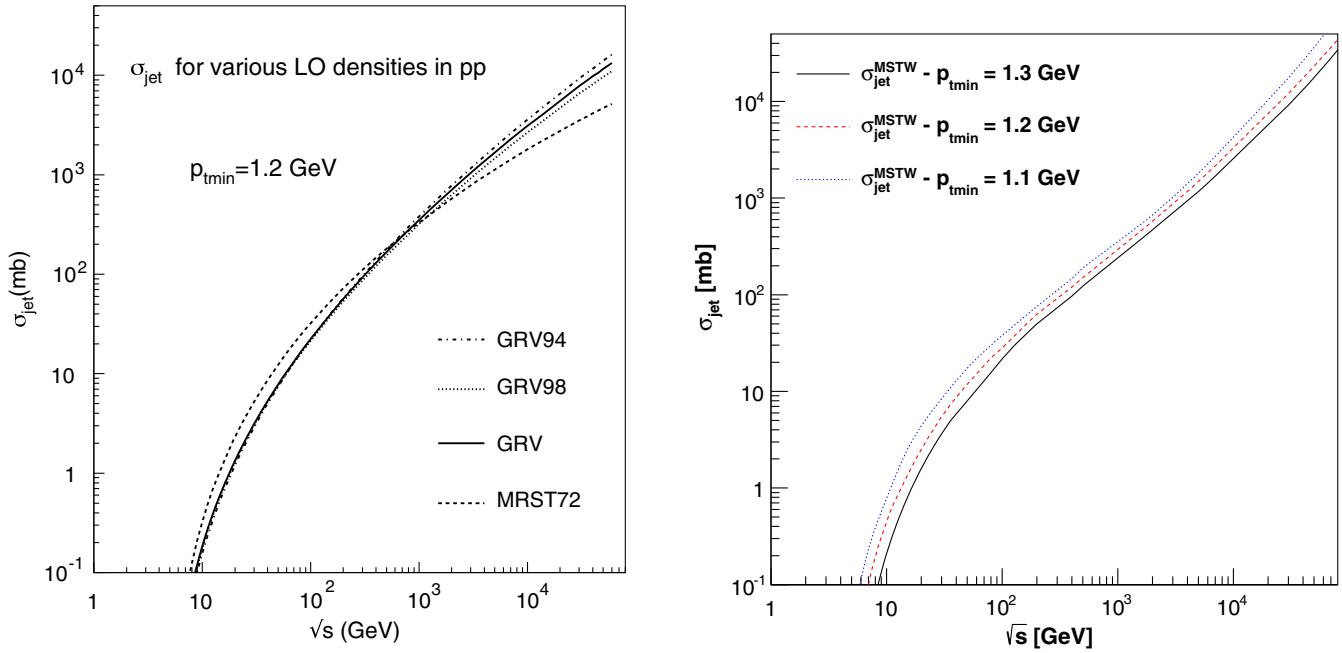

FIG. 1 (color online). Integrated minijet cross section for GRV (older) densities [8–10] or MRST72 [11] and a fixed chosen p_{tmin} value (left) and with MSTW2008 [12] LO PDFs (right) for a range of p_{tmin} values showing a distinct change of behavior, from a very fast rise to a power law, around $\sqrt{s} \simeq (10 \div 20)$ GeV.

III. SOFT GLUON RESUMMATION AND THE FROISSART BOUND

We now turn to the *second fact* mentioned earlier. In our model the softening of the rise is obtained by soft gluon emission, a phenomenon always accompanying hard scattering, such as the one which results in the minijet production. Our starting point is that resummed soft gluon emission tames the rise of the minijet cross section. Soft emission always decreases the observable cross section, since it introduces an overall transverse momentum $K_t \neq 0$ in the center of mass of the colliding particles; namely it leads to acollinearity of the initial particles in the scattering. We have suggested that soft gluon QCD resummation plays the same effect in hadron-hadron collisions, in particular accompanying hard parton-parton scattering. In Ref. [13], we advanced the conjecture that such a phenomenon is behind the initial decrease of total cross sections, before the onset of minijets. Past ISR, perturbative QCD effects, i.e. minijets, take over, and the combination of the decrease due to soft gluon resummation (SGR) and the rise of minijets transforms the rapid power law rise into a milder behavior, leading to the second important fact mentioned in Sec. II.

A quantitative description of this mechanism poses an extraordinary challenge, and we shall here briefly outline how we have approached the problem in our model [14].

We consider the following standard expression for soft k_t resummation, i.e.

$$\frac{d^2P(\mathbf{K}_t)}{d^2\mathbf{K}_t} = \frac{1}{(2\pi)^2}\int d^2\mathbf{b}\, e^{i\mathbf{K}_t\cdot\mathbf{b}} e^{-h(\mathbf{b})} \tag{5}$$

$$h(\mathbf{b}) = \int d^3\bar{n}(k)[1 - e^{-i\mathbf{k}_t\cdot\mathbf{b}}], \tag{6}$$

where $d^3\bar{n}(k)$ is the average number of soft quanta emitted during a collision. In our model, the Fourier transform of the above expression describes the impact parameter distribution of partons in the proton, $A(b,s)$, during the hard gluon-gluon collision. In the well-known formulation of SGR [15,16], the lower limit of the k_t integration is excluded, via an infrared cutoff of order Λ_{QCD}. This procedure is acceptable as long as there is no singularity in the infrared region [16], which is certainly not true when confinement effects play a role.

Our model relies on an adequate, albeit phenomenological, inclusion of *the infrared region*. We parametrize the very low k_t emission with a parameter p, through an effect of zero momentum or close to zero momentum emission. Our parametrization of the IR region has been discussed at length in many publications, see for instance Refs. [5] and [13], and will not be repeated here, except to remind the reader that it basically amounts to describing the IR region through a singular but integrable expression for the coupling α_{eff} of very soft, infrared gluons from the emitting quark current; namely we use

$$\alpha_{\rm eff} = \frac{12\pi}{33-2N_f}\frac{p}{\log[1+p(k_t/\Lambda_{\rm QCD})^{2p}]}. \quad (7)$$

The parameter p regulates the singularity; it is by construction $1/2 < p < 1$. We determine its value phenomenologically, but we expect it to be related to the coefficient of the beta function. With such an expression, k_t-resummation in the transverse momentum of soft gluons emission can be performed down into the $k_t = 0$ region.

We label the impact parameter distribution accompanying minijet scattering with the subscript BN as $A^{pp}_{BN}(p, PDF; b, s)$, pinpointing to the need for resummation of soft quanta emitted in the so-called infrared catastrophe [17]. We have

$$A^{pp}_{BN}(p, PDF; b, s) = \frac{e^{-h(p;b,s)}}{\int d^2\mathbf{b} e^{-h(p,b,s)}} \quad (8)$$

$$h(b,s;p) = \frac{16}{3\pi}\int_0^{q_{\rm max}} \frac{dk_t}{k_t}\alpha_{\rm eff}(k_t)\log\frac{2q_{\rm max}}{k_t}[1-J_0(bk_t)] \quad (9)$$

$$\alpha_{eff}(k_t) \propto (\frac{k_t}{\Lambda})^{-2p} \qquad k_t \to 0, \quad (10)$$

where the upper limit of integration $q_{\rm max}$ indicates the PDF dependence, as we see shortly. We have discussed the above distribution in many publications, starting with Ref. [14]. Its main characteristic is to include soft gluon resummation down to $k_t = 0$, and regulate the infrared singularity through a parameter p, so as to correspond to a dressed gluon potential $V \sim r^{2p-1}$ for $r \to \infty$. We have also shown an important consequence of an expression such as the above for $\alpha_{eff}(k_t \to 0)$ [18], namely that, asymptotically, the regularized and integrated soft gluon spectrum of Eq. (9) is seen to rise as

$$h(b,s;p) \to (b\bar{\Lambda})^{2p} \quad (11)$$

and the b-distribution A^{pp}_{BN} exhibits a cutoff in b-space strongly dependent on the parameter p. When the above distribution is included in an eikonal minijet model, such a cutoff is seen to give rise to a total cross section which rises asymptotically as $[\log s]^{1/p}$, as shown in Ref. [18], where details can be found.

Phenomenologically, just as the minijet cross section depends on the PDFs, so will the soft gluon spectrum accompanying the hard scattering, and so will the expression we propose for the impact parameter distribution of partons. This happens through the maximum transverse momentum allowed to single soft gluon emission during the hard gluon-gluon collision. The dynamical scale $q_{\rm max}(s)$ in Eq. (9) is obtained from the kinematics for single soft gluon emission [19]. In our model, as discussed in the original formulation [5], we have made some approximations, such as that most contributions come from $p_t \simeq p_{\rm tmin}$ and have taken averages over the densities chosen for the minijet cross section. Thus, we use the expression

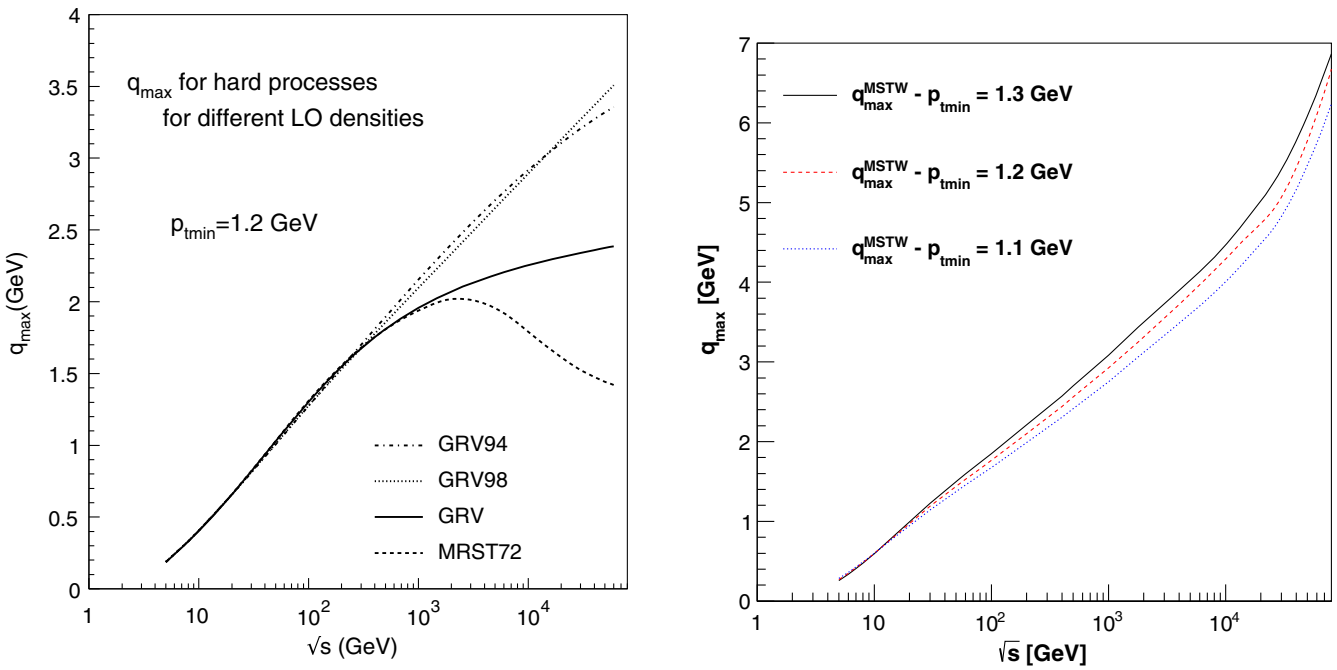

FIG. 2 (color online). Dynamically generated scale $q_{\rm max}$ for different PDFs and a fixed $p_{\rm tmin}$ value (left panel) and MSTW2008 LO parton densities, within a range of $p_{\rm tmin}$ values.

$$q_{\max}(s;p_{\rm tmin}) = \sqrt{\frac{s}{2}}\frac{\sum_{i,j}\int\frac{dx_1}{x_1}\int\frac{dx_2}{x_2}\int_{z_{\min}}^1 dz f_i(x_1)f_j(x_2)\sqrt{x_1x_2}(1-z)}{\sum_{i,j}\int\frac{dx_1}{x_1}\int\frac{dx_2}{x_2}\int_{z_{\min}}^1 dz f_i(x_1)f_j(x_2)} \tag{12}$$

with $z_{\min}=4p_{\rm tmin}^2/(sx_1x_2)$. This scale, the maximum transverse momentum allowed for single soft gluon emission at a given energy, has a strong dependence on the PDFs used for its calculation, and on $p_{\rm tmin}$, as well. In this paper we shall show results for different LO PDFs. In previous publications [3], we discussed the case of GRV [8–10], or MRST72 [11]. In the left panel of Fig. 2, we show the s-dependence of the soft energy scale $q_{\max}$ for these densities and for one fixed value of $p_{\rm tmin}$. New updated densities are now available, and we show in the right hand panel the s-dependence for a range of values for $p_{\rm tmin}$ and for the recent LO PDF set, MSTW2008, for brevity also called MSTW in this paper [12]. Thus, while the scale defining the minijet contribution, i.e. $p_{\rm tmin}$, is fixed, the model has a dynamically generated energy dependent scale, $q_{\max}$.

IV. ONE CHANNEL MINIJET MODEL FOR TOTAL, ELASTIC AND INELASTIC CROSS-SECTIONS

The appearance of minijets in hadronic collisions has a long history [20]. The construction of the total hadronic cross section with minijets started in Ref. [21] with a simple model with an energy dependent $p_{T\rm min}(s)$. The original suggestion in Ref. [21] did not use the eikonal representation and was based on phenomenologically determined values of $p_{T\rm min}(s)$ at different energies. Embedding the minijets in the eikonal formulation [22], unitarity would be automatically satisfied, but the modeling increased due to the request of specifying an impact parameter distribution. Durand and Pi's original suggestion and many others to follow use the one-channel description, but their use is limited, and in what follows we shall clarify these limitations.

Presently, good descriptions of all the components of the cross section are obtained through multichannel formulations. Some of them [23] are discrete *á la Good and Walker* [24], others are based on a continuous distribution of channels [25,26]. The price to pay then is the addition of more free parameters. Current models in perturbative QCD, on accounting for multiple Pomeron interactions, invoke enhanced "fan" diagrams [27–29] which require the knowledge of nonlinear coupling between Pomerons. Nonlinear equations such as the Balitsky–Kovchegov equation [30,31] are used to describe these nonlinear contributions to diffraction. Such nonlinear couplings become important when the gluon momentum becomes very small, a region insofar unreachable by perturbative QCD. Thus, while diffraction needs a multichannel approach, its complete description and phenomenology so far have to rely on more parameters [32], some of which embody the nonlinear behavior in the unknown infrared region.

In this section, we shall discuss the minijet contribution to total, elastic, and inelastic cross sections, using a one-channel eikonal formulation, and leave to a forthcoming publication the implementation to a general model and the inclusion of diffractive processes.

A. Total cross section

In this section we shall update our minijet model results to LHC13 energies and beyond. To construct the total cross section, minijets are embedded into the eikonal formulation. Starting with

$$\sigma_{\rm total}=2\int d^2\vec{b}[1-\Re e(e^{i\chi(b,s)})] \tag{13}$$

and neglecting the real part in the eikonal formulation at very high energy, the above expression further simplifies into

$$\sigma_{\rm total}=2\int d^2\vec{b}[1-e^{-\chi_I(b,s)}], \tag{14}$$

where $\chi_I(b,s)=\Im m\chi(b,s)$. Notice that $\Re e\chi(b,s)\simeq 0$ is a reasonable approximation for the scattering amplitude in **b**-space at $t=0$, where very large values of the impact parameter dominate and phenomenologically the ratio of the real to the imaginary part of the forward scattering amplitude $\rho(s)\ll 1$. By properly choosing a function $\chi_I(b,s)$, all total hadronic cross sections, pp, $p\bar{p}$, πp, etc., can be described up to currently available data [33]. In the vast majority of models, new data have often required an adjustment of the parameters which give $\chi_I(b,s)$.

In previous publications, we proposed a band of which the upper border gave a good prediction for LHC results. By updating the model and anchoring the parameter set to LHC results, one can now proceed to refine our predictions for higher energies, LHC13 and beyond, to the cosmic rays region. The eikonal function of the minijet model of Refs. [5,13] is given by

$$\begin{aligned}2\chi_I(b,s) &= n_{\rm soft}^{pp}(b,s)+n_{\rm jet}^{pp}(b,s)\\ &= A_{FF}(b)\sigma_{\rm soft}^{pp}(s)\\ &\quad + A_{BN}^{pp}(p,PDF;b,s)\sigma_{jet}(PDF,p_{\rm tmin};s).\end{aligned} \tag{15}$$

The first term includes collisions with $p_t\le p_{\rm tmin}\sim(1\div 1.5)$ GeV, and the second is obtained from the minijet cross section. The term $n_{\rm soft}^{pp}(b,s)$ is not predicted by our model so far, and we parametrize it here with $\sigma_{\rm soft}^{pp}(s)$, obtained with a constant and one or more decreasing terms, and A_{FF}, the impact parameter distribution in the

nonperturbative term, obtained through a convolution of two proton form factors.

As we have seen, the second term in Eq. (15) is numerically negligible at energies $\sqrt{s} \lesssim 10$ GeV. The perturbative, minijet, part discussed previously is defined with $p_t^{\text{parton}} \geq p_{\text{tmin}}$ and is determined through a set of perturbative parameters for the jet cross section, namely a choice of PDFs and the appropriate p_{tmin}. Since soft gluon resummation includes all-order terms in soft gluon emission, our model uses LO, library distributed, PDFs.

In our previous publications [2,3], we have reproduced data for pp and $\bar{p}p$, up to the TeVatron results. However, the large differences among the Tevatron measurements did not allow a precise description at higher energies, such as those at the LHC. Therefore, we have updated our analysis, using only pp data, ISR, and the recent LHC measurements, and including a more recent set of LO densities, MSTW2008 [12]. The values of p and p_{tmin} which better reproduce the LHC result are obtained by varying $p_{\text{tmin}} \simeq 1 \div 1.5$ GeV and $1/2 \lesssim p \lesssim 0.8$. The result, for the total pp cross sections, is shown in Fig. 3. The $\bar{p}p$ points are shown but have not been used for the phenomenological fit. Cosmic ray extracted values for pp have not been used either. We have included the curves corresponding to GRV densities and compared our model with other predictions [7,34,35]. Table I contains the points corresponding to our model results for both GRV and MSTW2008 densities. Results for MRST72 densities can be found in Ref. [36], together with details of different parameter sets used for the different PDFs. We notice that our model is able to describe very well all the total cross section accelerator data and gives a good agreement with cosmic ray data. The AUGER [37] point falls within the two different parameterizations we are using, a full line for MSTW and dashes for GRV. By construction, both parametrizations remain very close up to LHC7 and LHC8 energies and start diverging as the energy increases, as a consequence of the uncertainty on the very low-x behavior of the densities.

To summarize the results of this section, in the model we have proposed, past ISR energies minijets appear as hard gluon-gluon collisions accompanied by soft gluon emission k_t-resummed down into the infrared region. In this language, we have a *dressed* hard scattering process, with the minijet cross section giving the same energy behavior as the hard Pomeron, and soft gluon resummation providing *the dressing*, in which the hard interaction is embedded. The eikonal formulation then transforms this *dressed hard gluon* interaction into a unitary ladder. The main difference with other minijet models such as for instance in Ref. [41] is the taming mechanism ascribed to soft gluon resummation in the infrared region.

B. One-channel eikonal minijet models and the inelastic cross section

The inelastic total cross section is defined by subtraction from the total and the elastic cross sections. However, experimentally, it is usually defined only in specific phase space regions and eventually extrapolated via Monte Carlo simulation programs, which also include parameters and

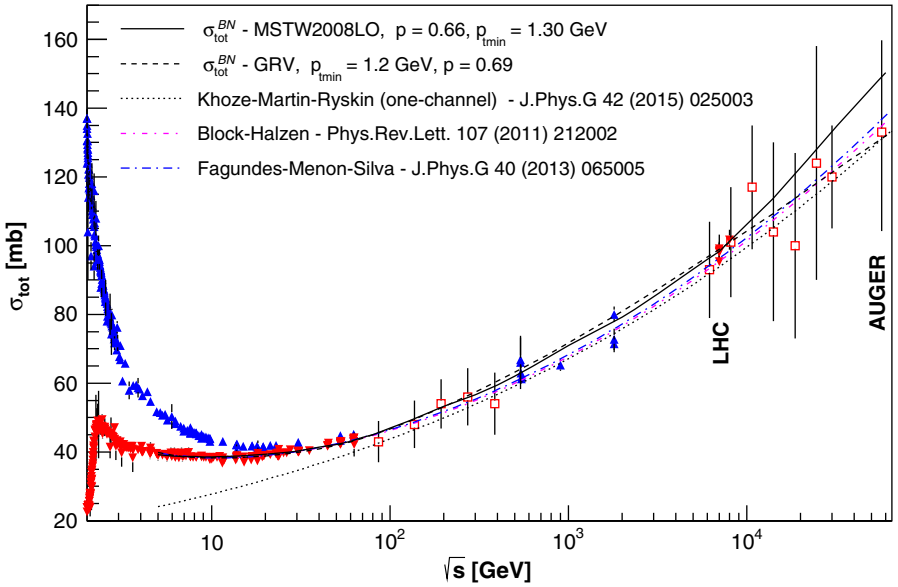

FIG. 3 (color online). QCD minijet with soft gluon resummation model and pp total cross section. Accelerator data at LHC include TOTEM [38,39] and ATLAS measurements [40]. Neither $\bar{p}p$ nor the cosmic ray data points have been used for the calculation. Our results are shown with predictions in the high cosmic ray region obtained with two types of densities, GRV and MSTW, and they are compared with one-channel model from Khoze *et al.* [7]. The red *dot-dashed* curve corresponds to fits to the total cross section by Block and Halzen [34], and the dot-dashed blue line represents the fit by Fagundes–Menon–Silva [35].

TABLE I. Total cross section values in mb, from the minijet model with two different PDFs sets.

$\sqrt{s}$ (GeV)	$\sigma_{\rm total}^{\rm GRV}$ (mb)	$\sigma_{\rm total}^{\rm MSTW}$ (mb)
5	39.9	39.21
10	38.2	38.6
50	41.9	42.2
500	63.2	62.0
1800	79.5	77.5
2760	85.4	83.6
7000	98.9	98.3
8000	100.9	101.3
13000	108.3	113.3
14000	109.3	113.7
57000	131.1	144.5

choice of models in the diffractive region. One exception is TOTEM which covers a large rapidity range. In this subsection, we shall focus on one, theoretically well-defined, part of the inelastic cross section, what we define as *uncorrelated*, which is appropriately described in the minijet context and through the one-channel mode. In the following we shall see how.

Since our study [3] on the inelastic cross section at the LHC, soon followed by the first experimental results [42], data related to measurements in different kinematic regions have appeared. Extensive and detailed measurements have been obtained for the inelastic proton-proton cross section by CMS [43], ATLAS [42], TOTEM [39,44], ALICE [45], and LHCb [46] collaborations. These measurements cover different regions, central and midrapidity, large rapidity, and high and low mass diffractive states. Extensive QCD modeling, including minijets [47–50], goes in describing the different regions.

Here, we consider the implication of any given one-channel eikonal model. Thus, we repeat the argument about the relation between the Poisson distribution of independent collisions and diffractive processes given in Ref. [3], where we stressed that the inelastic cross section in a one-channel eikonal model coincides with the sum of independently (Poisson) distributed collisions in b-space. Namely, with

$$\sigma_{\rm total} = \sigma_{\rm elastic} + \sigma_{\rm inel}, \tag{16}$$

then, in a one-channel (*one-ch*) mode,

$$\sigma_{\rm inel}^{\rm one\text{-}ch} \equiv \sigma_{\rm tot} - \sigma_{\rm elastic}^{\rm one\text{-}ch} = \int d^2\mathbf{b}[1 - e^{-2\chi_I(b,s)}]. \tag{17}$$

But since

$$\sum_1^\infty \frac{(\bar{n})^n e^{-\bar{n}(b,s)}}{n!} = 1 - e^{-\bar{n}(b,s)}, \tag{18}$$

one can identify the integrand at the right-hand side of Eq. (17) with a sum of totally independent collisions, with $2\chi_I(b,s) = \bar{n}(b,s)$. We suggest that this means that in so doing one excludes diffraction and other quasielastic processes from the integration in Eq. (17). Hence, the simple splitting of the total cross section as in Eq. (16) needs to be better qualified when a one-channel eikonal is used. In such a case, the "elastic" cross section

$$\sigma_{\rm elastic}^{\rm one\text{-}ch} = \int d^2\vec{b}|1 - e^{-\chi_I(b,s)}|^2 \tag{19}$$

must be including part of the inelastic contribution, i.e.

$$\sigma_{\rm elastic}^{\rm one\text{-}ch} = \sigma_{\rm elastic} + \text{diffractive or otherwise correlated processes}, \tag{20}$$

and $\sigma_{\rm inel}^{\rm one\text{-}ch}$ is only the nondiffractive part. Within this approach, we can compare Eq. (17) with data.

This comparison is shown in Fig. 4, where the present inelastic cross section data up to AUGER energies [37] are plotted. The blue band corresponds to the expectations from Eq. (17) where the same eikonal function $\chi_I(b,s)$ which gives the total cross section of Fig. 3 is used. Having anchored the eikonal $\chi_I(b,s)$ to the LHC total cross section, the band indicates the spread of predictions due to the different asymptotic low-x behavior of the employed

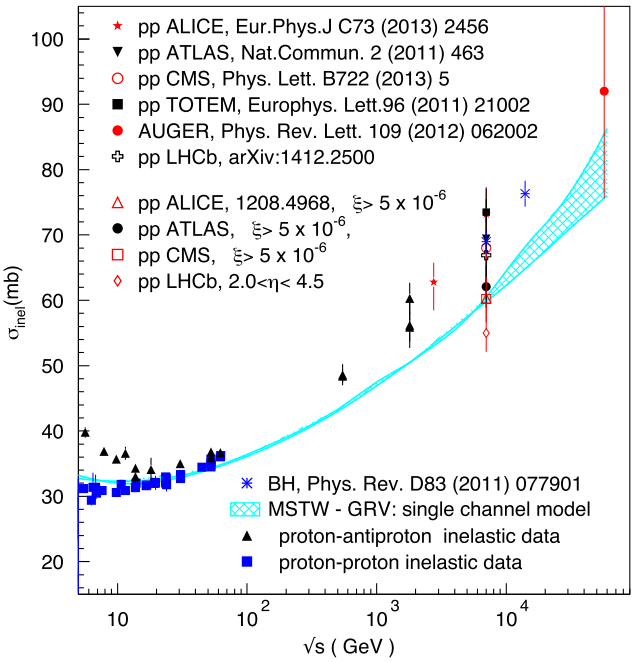

FIG. 4 (color online). Data for the inelastic cross section and comparison with GRV and MSTW2008 densities in the present one-channel minijet model. We also show comparison with Ref. [34].

densities, as the energy increases beyond LHC8. The top curve corresponds to MSTW2008, and the lower one corresponds to GRV.

The comparison with experimental data is very interesting. While the present LHC inelastic cross section data span a range of values corresponding to different kinematic regions, Eq. (17) identifies the region where uncorrelated events described by minijet collisions, parton-parton collision with $p_t > p_{\rm tmin}$, play the main role. From the comparison with data, we can identify it with the region $\xi = M_X^2/s \geq 5 \times 10^{-6}$ where three LHC experiments, ATLAS [42], CMS [43], and ALICE [45], agree to a common value within a small error. This measurement is in the high mass region (for instance, at LHC7 the lower bound gives $M_X = 15.7$ GeV). LHCb results correspond to a lower cross section, but they do not cover the same region of phase space.

The results of this and of the previous subsection are summarized in Fig. 5 where the bands correspond to different PDFs used in the calculation of minijets and to their different extrapolation to very low x at the cosmic ray energies.

The dashed yellow band is the one-channel inelastic cross section that only includes Poisson-distributed independent scatterings. That is, once the parameters of the eikonal $\chi(b,s)$ are chosen to give an optimal reproduction of the total cross section, the computed inelastic cross section immediately gives the uncorrelated part of the total inelastic cross section. The importance of this fact for cosmic ray deduced pp cross sections has been noticed in Ref. [36] and shall be examined further elsewhere.

C. Diffractive, elastic, and inelastic cross sections reexamined

The total cross section, which our model successfully describes, includes different components, but only one of them is well defined experimentally as well as theoretically; that is the elastic cross section. It is well known that one-channel eikonal models fail to simultaneously describe the total and the elastic cross section through the entire available c.m. energy range, with the same parameter set. In the last subsection, we delineated this shortcoming through the observation that, once minijets become operative past the soft edge, the computed elastic cross section includes correlated inelastic collisions, and the computed inelastic lacks the same (i.e., its correlated inelastic part). We now discuss this matter in detail so as to make these statements quantitative. We shall do so through the one-channel minijet model with a suitable parametrization of diffractive data.

In one-channel eikonal models, with the inelastic part given by Eq. (17), the elastic part of the total cross section is given by Eq. (19). Notice that, whereas Eq. (17) is exact, in Eq. (19) the real part of the eikonal function has been neglected, as in Eq. (13).

Equation (19) reproduces with a good approximation the elastic cross section data up to the onset of minijets, deviating significantly from the data already at energies 100 GeV. In particular, at the Tevatron, Eq. (19) gives an elastic cross section roughly 30% higher than the data. This is shown in the left-hand plot of Fig. 6, where the one-channel result from Eq. (19) is plotted together with elastic scattering data and an empirical parametrization of all

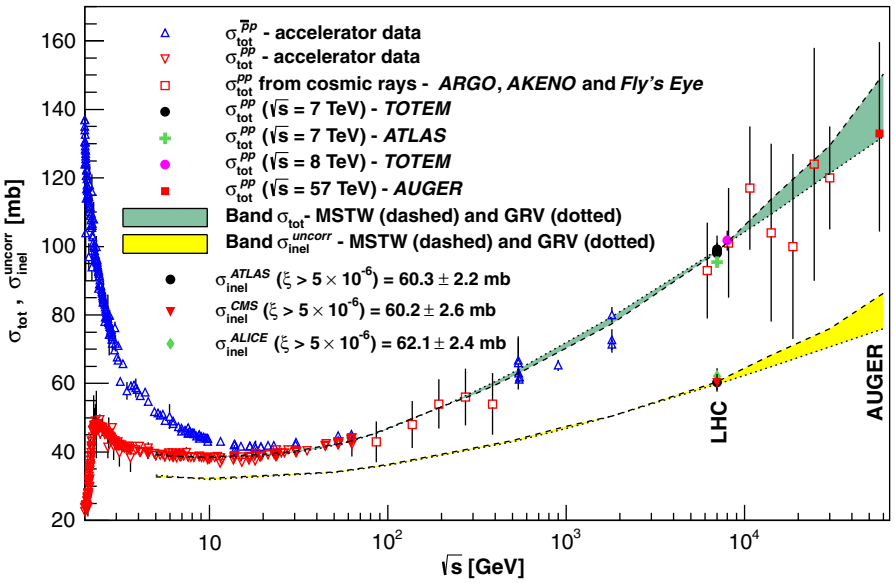

FIG. 5 (color online). Results for our eikonalized QCD minijet with the soft gluon resummation model are shown for the pp total cross section and for the inelastic uncorrelated part of the inelastic cross section. Accelerator data at the LHC include TOTEM [38,39] and ATLAS measurements [40]. The inelastic uncorrelated cross section is compared with inelastic processes for $M_X^2/s > 5\times10^{-6}$ as measured by ATLAS [42], CMS [43], and ALICE [45]. The green and yellow bands give the uncertainty following the use of different PDFs sets, MSTW2008 and GRV.

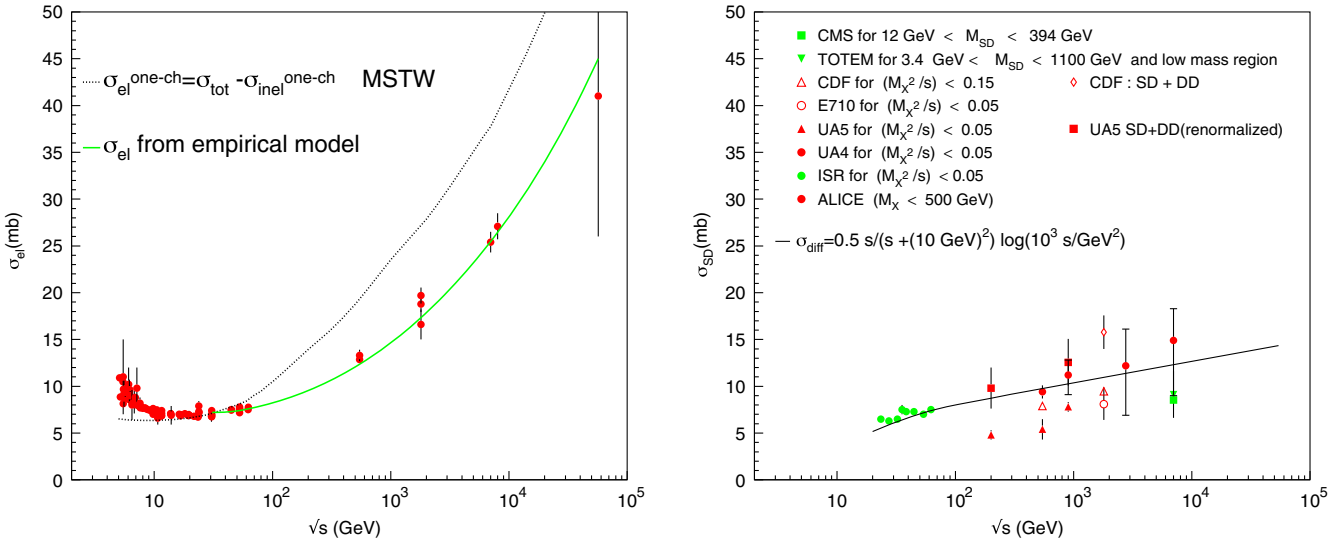

FIG. 6 (color online). At left, we show the elastic pp cross section from the one-channel mode given by the dotted curve, with the choice of the MSTW2008 PDF as in the upper curve of Fig. 3. The green curve corresponds to an empirical parametrization of all differential elastic pp data [51]. Comparison is done with both pp and $p\bar{p}$ data. The right-hand panel shows diffraction data from E710 [53], UA5 [54,55], UA4 [56], ISR [57], CDF [58], CMS [59], TOTEM [39], and ALICE [45] compared with the parametrization given by Eq. (23) mentioned in the text.

elastic differential cross section pp data from ISR to LHC7 [51]. This parametrization leads to the expression

$$\sigma_{\text{elastic}} = At_0 e^{Bt_0} E_8(Bt_0) + \frac{C}{D} + 2\sqrt{AC}\cos\phi t_0 e^{(B+D)t_0/2} E_4\left(\frac{(B+D)t_0}{2}\right), \tag{21}$$

where

$$E_n(x) = \int_1^\infty \frac{e^{-xy}}{y^n} dy. \tag{22}$$

The model of Ref. [51] is based on the well-known Phillips and Barger model [52] for the elastic differential cross section, implemented by a form factor term to fully reproduce the optical point, and hence the total cross section, as well as the forward slope. Through suitable predictions for the high energy behavior of the parameters, the parametrization of Ref. [51] provides a model independent prediction both for elastic and total cross sections at very high energies and hence can be used as a good test of different models in the high energy region beyond present accelerator data.

The plot at the left-hand of Fig. 6 shows that at low energies, before the onset of mini-jets, one-channel models may be used to describe both elastic and total cross-sections. However, past ISR energies the threshold of perturbative QCD, reflected in the appearance of the *soft edge*, is crossed, and one-channel models fail. One-channel models are also unable to reproduce the behavior of the differential elastic cross section, and multichannel models with added parameters are then needed to describe diffraction. The difficulty with proper descriptions of diffraction is that, at different energies, different parts of the phase space are accessed by different experimental setups, as we show in the right-hand plot of Fig. 6. For the argument to follow, we consider an estimate of σ_{Diff} given by Eq. (36) of Ref. [60], which provides a good interpolation of single diffractive (SD) data, from ISR to the LHC results from ALICE, CMS, and TOTEM, as we shown in Fig. 6, i.e.

$$\sigma_{\text{Diff}}(s) = \left[\frac{(0.5\text{ mb})\text{ s}}{s + (10\text{ GeV})^2}\right] \log\left(\frac{10^3\text{ s}}{\text{GeV}^2}\right). \tag{23}$$

We have adopted this parametrization for the full diffractive component at high energy. This is an approximation, justified at very high energy by the TOTEM result for double diffraction (DD) [61], namely $\sigma_{DD} \simeq 0.1$ mb, although this result was obtained in a narrow range of pseudorapidity and more data are needed to conclude that DD does not play a significant role at LHC energies. At lower energy the definitions vary, as we show in this figure.

We shall now show how the one-channel minijet model presented here can be used to predict the full inelastic cross section at higher energies.

We start with the elastic cross section and consider now the difference

$$\sigma_{\text{elastic}}^{\text{one-ch}} = \sigma_{\text{tot}} - \sigma_{\text{inel}}^{\text{one-ch}}, \tag{24}$$

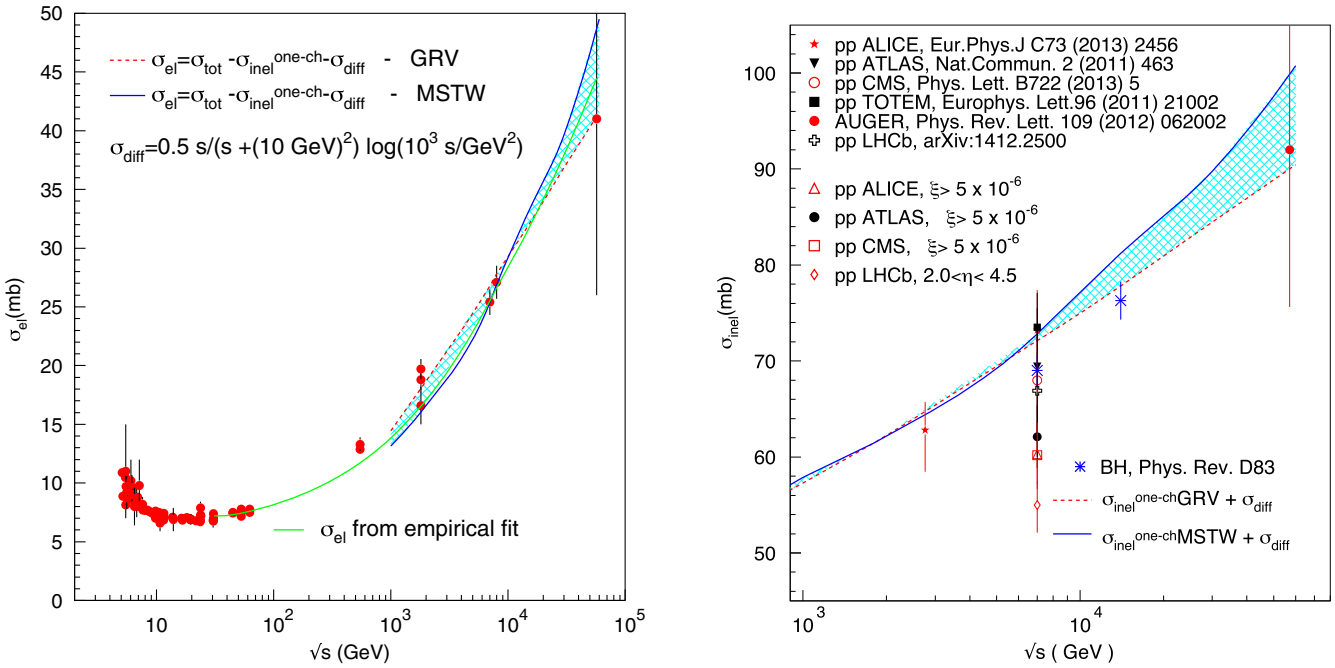

FIG. 7 (color online). Left panel: the total elastic cross section obtained by subtracting single diffractive contributions, indicated as $\sigma_{\rm diff}$, from the one-channel model result. The resulting curve is compared with pp and $p\bar{p}$ data and the empirical parametrization of Ref. [51], which is seen to fall within the two model predictions. The right panel shows the corresponding exercise for the inelastic cross section: at high energies, adding diffraction brings the one-channel result in agreement with data.

which includes the diffractive (otherwise said, correlated inelastic) contribution, as also discussed in general terms in Ref. [62], among others. If

$$\sigma_{\rm inel} = \sigma_{\rm inel}^{\rm one\text{-}ch} + \sigma_{\rm Diff}, \tag{25}$$

then we should be able to obtain the measured elastic cross section from

$$\sigma_{\rm elastic} = \sigma_{\rm elastic}^{\rm one\text{-}ch} - \sigma_{\rm Diff}. \tag{26}$$

We compare the procedure outlined through Eqs. (23) and (26) with experimental data and with the empirical parametrization of Eq. (21). The result is shown in the left panel of Fig. 7. We see that such a procedure gives a good description of the elastic cross section at high energy, basically past the CERN $Sp\bar{p}S$.

TABLE II. Minijet model predictions for the inelastic cross section at $\sqrt{s} = 13$ TeV. Predictions of $\sigma_{\rm inel}$ in the full phase space were obtained by adding $\sigma_{\rm diff}(13\ {\rm TeV}) = 12.9$ mb to $\sigma_{\rm inel}^{\rm uncorr} \equiv \sigma_{\rm inel}^{\rm one\text{-}ch}$.

PDF	$\sigma_{\rm inel}^{\rm uncorr}$ (mb)	$\sigma_{\rm inel}$ (mb)
GRV	64.3	77.2
MSTW	68.1	81.0

Likewise, from Eq. (25), we can see that, by adding the diffractive part, parametrized as in Eq. (23), to the prediction from the one-channel model, it is possible to obtain a good description of the high energy behavior of the inelastic cross section. This is shown in the right-hand panel of Fig. 7. It must be noticed that this procedure shows agreement with data only past ISR energies (in fact from $Sp\bar{p}S$ onward) and that a model describing both the low and the high energy will have to go beyond the one-channel exercise described here. In Table II, we show the predictions from this model for the inelastic cross section at LHC13, $\sqrt{s} = 13$ TeV.

The result of this subsection confirms the interpretation that at high energies, past the beginning of the rise and the onset of minijets, the one-channel inelastic cross section is devoid of most of the diffractive contribution.

V. SUMMARY AND CONCLUSIONS

We have shown that the onset and rise of the minijet cross section provide the dynamical mechanism behind the appearance of a soft edge [1], i.e., a threshold in the total cross section around $\sqrt{s} \simeq (10 \div 20)$ GeV. Thus, our model for the total pp cross section that utilizes minijets with soft-gluon resummation has a built in soft edge. It has been updated with recent PDFs for the LHC at $\sqrt{s} = 7$, 8 TeV and predictions made for higher energy LHC data and cosmic rays.

We have also discussed in detail the reasons behind failures to obtain correct values for the elastic cross sections from a one-channel eikonal that obtains the total cross section correctly. It has been shown, through the use of phenomenological descriptions of diffractive (otherwise said, correlated inelastic) cross sections, that a one-channel elastic cross section is indeed a sum of the true elastic plus correlated inelastic cross sections. An application of this fact to cosmic ray data analysis for the extraction of pp uncorrelated-inelastic cross sections shall be presented elsewhere.

ACKNOWLEDGMENTS

We thank Simone Pacetti for collaboration about the empirical model results. A. G. acknowledges partial support by Junta de Andalucia (Grants No. FQM 6552 and No. FQM 101). D. A. F. acknowledges the São Paulo Research Foundation and CAPES for financial support (Contract No. 2014/00337-8). O. S. acknowledges partial support from funds of Foundation of Polish Science Grant No. POMOST/2013-7/12, that is cofinanced from the European Union, Regional Development Fund.

[1] M. M. Block, L. Durand, F. Halzen, L. Stodolsky, and T. J. Weiler, Phys. Rev. D **91**, 011501 (2015).
[2] A. Achilli, R. M. Godbole, A. Grau, R. Hegde, G. Pancheri, and Y. Srivastava, Phys. Lett. B **659**, 137 (2008).
[3] A. Achilli, Y. Srivastava, R. Godbole, A. Grau, G. Pancheri, and O. Shekhovtsova, Phys. Rev. D **84**, 094009 (2011).
[4] J. L. Rosner, Phys. Rev. D **90**, 117902 (2014).
[5] A. Grau, G. Pancheri, and Y. Srivastava, Phys. Rev. D **60**, 114020 (1999).
[6] E. Gotsman, E. Levin, and U. Maor, Phys. Lett. B **716**, 425 (2012).
[7] V. Khoze, A. Martin, and M. Ryskin, J. Phys. G **42**, 025003 (2015).
[8] M. Gluck, E. Reya, and A. Vogt, Z. Phys. C **53**, 127 (1992).
[9] M. Gluck, E. Reya, and A. Vogt, Z. Phys. C **67**, 433 (1995).
[10] M. Gluck, E. Reya, and A. Vogt, Eur. Phys. J. C **5**, 461 (1998).
[11] A. D. Martin, R. G. Roberts, W. J. Stirling, and R. S. Thorne, Eur. Phys. J. C **4**, 463 (1998).
[12] A. Martin, W. Stirling, R. Thorne, and G. Watt, Eur. Phys. J. C **63**, 189 (2009).
[13] R. M. Godbole, A. Grau, G. Pancheri, and Y. N. Srivastava, Phys. Rev. D **72**, 076001 (2005).
[14] A. Corsetti, A. Grau, G. Pancheri, and Y. N. Srivastava, Phys. Lett. B **382**, 282 (1996).
[15] Y. L. Dokshitzer, D. Diakonov, and S. I. Troian, Phys. Lett. B **79**, 269 (1978).
[16] G. Parisi and R. Petronzio, Nucl. Phys. **B154**, 427 (1979).
[17] F. Bloch and A. Nordsieck, Phys. Rev. **52**, 54 (1937).
[18] A. Grau, R. M. Godbole, G. Pancheri, and Y. N. Srivastava, Phys. Lett. B **682**, 55 (2009).
[19] P. Chiappetta and M. Greco, Phys. Lett. B **106**, 219 (1981).
[20] G. Pancheri and Y. Srivastava, Phys. Lett. B **B159**, 69 (1985).
[21] T. K. Gaisser and F. Halzen, Phys. Rev. Lett. **54**, 1754 (1985).
[22] L. Durand and H. Pi, Phys. Rev. D **40**, 1436 (1989).
[23] V. Khoze, A. Martin, and M. Ryskin, Eur. Phys. J. C **74**, 2756 (2014).
[24] M. Good and W. Walker, Phys. Rev. **120**, 1857 (1960).
[25] P. Lipari and M. Lusignoli, Phys. Rev. D **80**, 074014 (2009).
[26] P. Lipari and M. Lusignoli, Eur. Phys. J. C **73**, 2630 (2013).
[27] M. Ryskin, A. Martin, and V. Khoze, Eur. Phys. J. C **72**, 1937 (2012).
[28] E. Gotsman, E. Levin, and U. Maor, Phys. Rev. D **85**, 094007 (2012).
[29] S. Ostapchenko, Phys. Rev. D **83**, 014018 (2011).
[30] I. Balitsky, Nucl. Phys. **B463**, 99 (1996).
[31] Y. V. Kovchegov, Phys. Rev. D **64**, 114016 (2001).
[32] S. Ostapchenko, Phys. Rev. D **81**, 114028 (2010).
[33] A. Grau, G. Pancheri, O. Shekhovtsova, and Y. N. Srivastava, Phys. Lett. B **693**, 456 (2010).
[34] M. M. Block and F. Halzen, Phys. Rev. D **83**, 077901 (2011).
[35] D. A. Fagundes, M. J. Menon, and P. V. R. G. Silva, J. Phys. G **40**, 065005 (2013).
[36] D. Fagundes, A. Grau, G. Pancheri, Y. Srivastava, and O. Shekhovtsova, Eur. Phys. J. Web Conf. **90**, 03002 (2015).
[37] P. Abreu *et al.* (Pierre Auger Collaboration), Phys. Rev. Lett. **109**, 062002 (2012).
[38] G. Antchev *et al.* (TOTEM Collaboration), Phys. Rev. Lett. **111**, 012001 (2013).
[39] G. Antchev *et al.* (TOTEM Collaboration), Europhys. Lett. **101**, 21004 (2013).
[40] G. Aad *et al.* (ATLAS Collaboration), Nucl. Phys. **B889**, 486 (2014).
[41] A. Giannini and F. Duraes, Phys. Rev. D **88**, 114004 (2013).
[42] G. Aad *et al.* (ATLAS Collaboration), Nat. Commun. **2**, 463 (2011).
[43] S. Chatrchyan *et al.* (CMS Collaboration), Phys. Lett. B **722**, 5 (2013).
[44] G. Antchev *et al.* (TOTEM Collaboration), Europhys. Lett. **101**, 21003 (2013).
[45] B. Abelev *et al.* (ALICE Collaboration), Eur. Phys. J. C **73**, 2456 (2013).
[46] R. Aaij *et al.* (LHCb collaboration), J. High Energy Phys. 02 (2015) 129.
[47] S. Ostapchenko, Phys. Rev. D **89**, 074009 (2014).
[48] S. Ostapchenko, Phys. Rev. D **74**, 014026 (2006).
[49] A. K. Kohara, E. Ferreira, and T. Kodama, J. Phys. G **41**, 115003 (2014).
[50] K. Goulianos, Eur. Phys. J. Web Conf. **71**, 00050 (2014).
[51] D. A. Fagundes, A. Grau, S. Pacetti, G. Pancheri, and Y. N. Srivastava, Phys. Rev. D **88**, 094019 (2013).

[52] R. Phillips and V. D. Barger, Phys. Lett. B **46**, 412 (1973).
[53] N. A. Amos *et al.* (E710 Collaboration), Phys. Lett. B **301**, 313 (1993).
[54] R. Ansorge *et al.* (UA5 Collaboration), Z. Phys. C **33**, 175 (1986).
[55] G. Alner *et al.* (UA5 Collaboration), Phys. Rep. **154**, 247 (1987).
[56] D. Bernard *et al.* (UA4 Collaboration), Phys. Lett. B **186**, 227 (1987).
[57] J. Armitage *et al.*, Nucl. Phys. **B194**, 365 (1982).
[58] T. Affolder *et al.* (CDF Collaboration), Phys. Rev. Lett. **87**, 141802 (2001).
[59] D. Dutta on behalf of (CMS Collaboration), arXiv: 1412.4977.
[60] R. Engel and R. Ulrich, Internal Pierre Auger Note GAP-2012, 2012.
[61] G. Antchev *et al.* (TOTEM Collaboration), Phys. Rev. Lett. **111**, 262001 (2013).
[62] B. Kopeliovich, Phys. Rev. C **68**, 044906 (2003).